Magnetite exsolution in almandine garnet

A. J. Brearley and P. E. Champness

Department of Geology, The University, Manchester, M13 9PL

ABSTRACT. Three almandine-rich metamorphic garnets have been studied by analytical electron microscopy and electron microprobe analysis. Electron microprobe analyses with total Fe calculated as Fe^{2+} show that there are no significant departures from stoichiometry due to the presence of Fe^{3+} in any of the garnets studied. However, in the transmission electron microscope (TEM) all the garnets were found to contain myriad spherical, iron-rich particles up to 400 Å in diameter. Microdiffraction techniques have revealed that the particles are a cubic spinel phase, consistent with magnetite. There is no crystallographic relationship between the host garnet and the particles, a rare situation for exsolution processes. The presence of such particles is interpreted in terms of the exsolution of magnetite from almandine garnet during cooling. This can apparently occur at temperatures below 550 °C. The size of the particles is a qualitative indicator of the cooling rate of the rock, but is also dependent on the original Fe^{3+} content of the host garnet.

KEYWORDS: magnetite, almandine, garnet, exsolution, transmission electron microscopy.

THE exsolution of oxide minerals is a common phenomenon in many silicate phases. Several examples of such exsolution have been successfully studied by transmission electron microscopy (TEM). Various authors have investigated exsolved oxide phases such as ilmenite and magnetite in olivines and pyroxenes, e.g. Moseley (1981, 1984), and recently Mongkoltip and Ashworth (1983) have discussed the exsolution of rutile and ilmenite from hornblende. In all the above examples the presence of a secondary exsolved, opaque phase had been initially observed by conventional light microscopy. The further use of TEM enabled detailed crystallographic, morphological and, in some cases, chemical information to be obtained in order to deduce a possible mechanism for the exsolution process. In contrast to the examples above, the present paper is concerned with the exsolution of magnetite particles from almandine garnet on a scale which is well beyond the resolution of the light microscope.

Sample descriptions

Three samples have been used for this study. All are from pelitic metamorphic rocks with differing metamorphic histories. Sample localities and petrography are presented below.

Sample RM5020 is a pelitic gneiss from the Moine inlier on the Ross of Mull, Isle of Mull, Scotland and has been studied in detail by Brearley (1984). The rock contains the assemblage garnet + biotite + muscovite + plagioclase + quartz. Garnet is abundant, occurring as small crystals less than 500 μm in diameter. The core regions are optically homogeneous (fig. 1a) and are separated from the outer inclusion-free rim of the garnet by a zone full of inclusions, dominantly quartz with subordinate opaques. These distinct zones are probably attributable to periods of growth at different rates during the metamorphic evolution of the area. The calculated conditions of formation for this rock are 550 ± 50 °C and 6–7 ± 1 kbar (Brearley, 1984).

Sample RM5001 is a high-grade pelitic hornfels from the contact aureole of the Ross of Mull granite. The detailed petrography has also been investigated by Brearley (1984) and the P–T conditions of formation have been determined as 700 ± 25 °C and 3.8 ± 0.3 kb. The hornfels contains the assemblage garnet–cordierite–biotite–sillimanite – andalusite – K-feldspar – plagioclase – quartz. Sillimanite occurs both as prismatic crystals intergrown with andalusite in the manner described by Bosworth, 1910 (see also MacKenzie and Guilford, 1981, p. 15), and as dense mats of fibrolitic sillimanite. Garnets which grew during the regional metamorphic event have been extensively resorbed and are rimmed by cordierite that formed by the reaction: garnet + sillimanite + quartz = cordierite. In the same rock, frequently within the same thin section, groups of new, euhedral, 'thermal' garnets up to 3 mm in diameter have grown during the contact metamorphism and typically have inclusion-filled cores (fig. 1b). These new contact garnets were selected for study by TEM.

The third sample, RAS1, is a pelitic schist from the base of the Ben Lui schist, Middle Dalradian, where it outcrops at Ben Challum, Tyndrum. The mineral assemblage in this rock consists of chloritoid–staurolite–garnet–margarite–paragonite–muscovite–chlorite–plagioclase–quartz.

The garnet porphyroblasts are large, up to 5 mm in diameter, and frequently contain curved inclusion trails of quartz, white mica, chloritoid and staurolite (fig. 1c). The $P-T$ conditions of this rock have not been determined, but it lies within the garnet zone of the Dalradian and probably reached 5 kbar and 535 °C (Atherton, 1977).

Electron microprobe analysis

Several garnets from each of the specimens have been extensively sampled by automated electron microprobe. All the analyses were carried out on a Cameca Camebax instrument fitted with a Link Systems energy dispersive spectrometer. The instrument was operated throughout at an accelerating voltage of 15 kV using a specimen current of 15 nA. Calibration of the machine was carried out using a variety of mineral and pure metal standards. Si, Al, Fe, Mn, Mg, and Ca were all analysed by ED spectrometry with Cr determined simultaneously using a wavelength dispersive spectrometer. Full ZAF corrections were applied to all the data. Representative core and rim analyses are shown in Table I. Cr was not detected in any of the samples and is therefore not reported.

Table I. Electron microprobe analyses of garnets

	1 Rim	2 Core	3 Rim	4 Core	5 Rim	6 Core
SiO_2	36.83	37.19	37.70	36.51	38.49	37.39
Al_2O_3	20.37	20.67	21.75	20.91	21.51	20.83
FeO	33.75	35.82	32.97	21.99	31.87	31.82
MnO	3.74	2.01	4.82	13.21	1.14	2.99
MgO	2.03	2.84	2.23	0.86	3.93	2.23
CaO	2.62	2.33	2.11	6.27	4.37	5.35
Total	99.45	100.87	100.09	99.75	101.32	100.65
Formula calculated on the basis of 12 [O] atoms						
Si	3.006	2.989	2.971	2.969	3.015	2.994
Al	1.960	1.958	2.030	2.004	1.986	1.966
Fe	2.304	2.408	2.232	1.495	2.088	2.131
Mn	0.259	0.137	0.331	0.910	0.076	0.203
Mg	0.247	0.341	0.269	0.105	0.459	0.267
Ca	0.229	0.200	0.183	0.474	0.367	0.459
	3.047	3.085	3.015	3.056	2.990	2.985
Garnet end-members						
Alm	75.82	78.06	74.03	48.72	69.62	68.68
Spess	8.51	4.45	10.98	29.77	2.51	6.74
Pyr	8.13	11.02	6.07	3.43	15.31	11.92
Gross	7.54	6.50	6.07	17.86	12.23	8.86

Analyses 1 and 2 – sample RM5020
Analyses 3 and 4 – sample RM5001
Analyses 5 and 6 – sample RAS1

FIG. 1. Garnet photomicrographs. (a) Regional garnet (RM5020) from Moinian pelitic gneisses, Ross of Mull, Mull. (b) Euhedral contact garnet (RM5001) from the inner aureole of the Ross of Mull granite, Isle of Mull, Scotland. (c) Regional metamorphic garnet (RAS1) from the Ben Lui schist, Ben Challum, Tyndrum, Scotland. The inclusion trails consist of quartz, white mica, chloritoid and staurolite. All in plane polarized light.

Results

RM5020. The analytical profile across a typical regional metamorphic garnet is shown in fig. 2. The core profiles for Fe, Mn, and Mg are very variable, but the compositional profile for Ca is completely
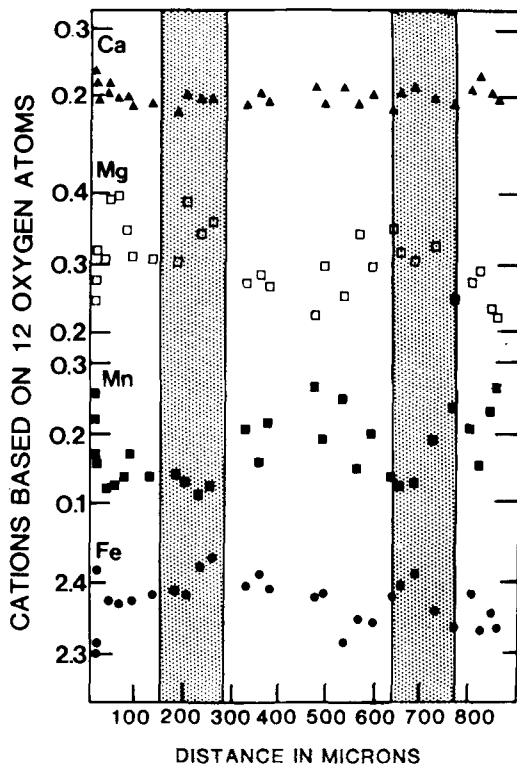
FIG. 2. Rim to rim compositional profile across a regional metamorphic garnet from the Ross of Mull inlier (RM5020) in terms of cations per formula unit based on 12[O] atoms. Zone of inclusions is shaded.

Mn and Ca show strong enrichment in the cores and are depleted towards the rims, with Fe and Mg exhibiting the inverse relationship. Mn is strongly enriched at the very edge of garnet and Fe and Mg depleted in a similar manner to that observed in the previous example (RM5020).
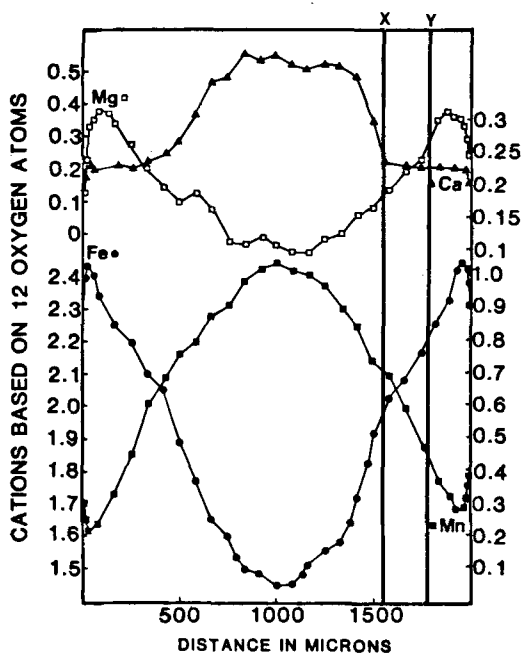
FIG. 3. Rim to rim compositional profile across a contact metamorphic garnet from the inner aureole of the Ross of Mull granite (RM5001) in terms of cations per formula unit based on 12[O] atoms. Points X and Y show the limits of the occurrence of magnetite particles within the garnet.

flat across the whole garnet, except for a slight decrease at the rim. All the other elements exhibit a slight asymmetry. Away from the core region there is a decrease in Mn and a corresponding increase in Fe and Mg which coincides with the zone of inclusions in the garnet. Towards the rim Fe and Mg increase and then drop rapidly at the very edge of the crystal with Mn displaying an antipathetic relationship. The reversal in this zoning pattern in the last 50 μm up to the rim (Mn increases rapidly) is a common feature of metamorphic garnets and is widely attributed to retrograde growth during cooling.

RM5001. The compositional profiles from the contact metamorphic garnets are substantially different from those observed in the regional garnets. An example is presented in fig. 3 for the major elements Fe, Mn, Mg, and Ca as cations based on 12 oxygen atoms per formula unit. The bell-shaped compositional profile found in this sample is typical of contact metamorphic garnets reported by several authors, e.g. Hollister (1969).

RAS1. The profiles from a large porphyroblastic garnet are illustrated in fig. 4 and are comparatively simple. Mn and Ca are slightly enriched in the cores and become depleted towards the rims, although the Ca profile is rather poorly defined in comparison with that for Mn. Fe and Mg display the characteristic inverse relationship. There is also a small increase in Mn at the very edge of the garnet coupled with a decrease in Mg.

Transmission electron microscopy

Experimental

Selected garnets from each of the three specimens were prepared for the TEM by conventional ion-bombardment techniques described by Barber

(1970) and Champness and Lorimer (1971) using Edwards IBMA1 and Iontech Microlap thinners. All the samples were studied in a Philips EM400T transmission electron microscope fitted with an EDAX 9100 energy dispersive spectrometer. All the observations were made at an operating voltage of 100 kV. A double-tilt goniometer specimen holder fitted with a beryllium insert to minimize extraneous X-ray generation was used throughout.
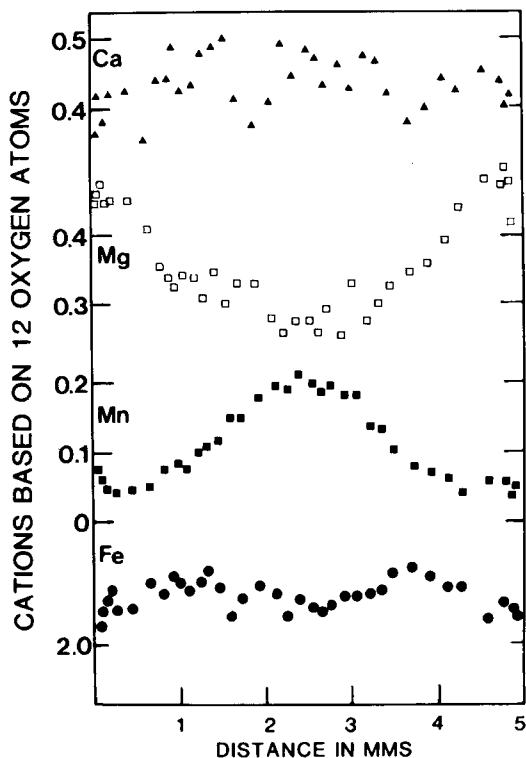
FIG. 4. Rim to rim compositional profile across a regional metamorphic garnet (RAS1) from the Ben Lui schist, Ben Challum, Tyndrum, Scotland, in terms of cations per formula unit based on 12[O] atoms.

Observations

RM5020. At low magnifications thin regions of the garnets from this sample appeared to be completely homogeneous, except for occasional inclusions of rutile up to 10 μm in size. However, at higher magnifications evidence of a microstructure was observed. Small particles, (fig. 5) roughly circular in shape (spherical in three dimensions) with diameters between 120 and 280 Å, were observed within the garnet matrix in all the compositional zones identified by EPMA. The distribu-

tion of this second phase appears to be random and has a particle density of $\sim 1.8 \times 10^{15}$ per cm^3 determined from the number of particles within a given area of thin foil. A foil thickness of 0.1 μm was assumed and gives a resultant volume fraction of approximately 0.75%
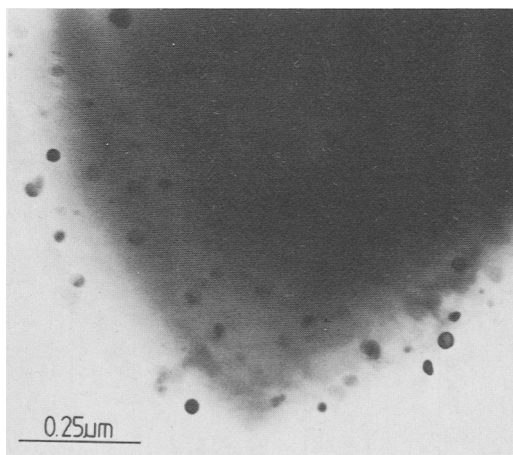
FIG. 5. Transmission electron micrograph of a region of garnet (RM5020) containing abundant spherical second phase particles.

At the edges of the thin foils preferential thinning of the garnet has taken place leaving the second phase particles standing out. Some particles appear to have a narrow rim which exhibits slightly different diffraction contrast from the rest of the particle. This is probably due to a thickness effect within the particle.

Electron diffraction indicates that there is no orientation relationship between the host garnet and the particles. Where the distribution of particles is most dense it is possible to obtain a very weak ring pattern superimposed on the garnet pattern. However, this powder pattern is not strong enough to enable the second phase particles to be identified unequivocally; their volume fraction within the garnet is too small to make any significant contribution to an electron diffraction pattern.

In order to obtain diagnostic diffraction data from the particles it was necessary to use microdiffraction techniques. Instead of using parallel illumination to obtain the diffraction pattern, as in selected area electron diffraction, microdiffraction uses a highly convergent, focused electron probe. Any diffraction effects are produced from the small volume of material covered by the probe. The

resolution of microdiffraction is somewhat higher than that obtainable when carrying out quantitative X-ray microanalysis in the TEM. The latter is limited to about 200 Å in diameter, because of the requisite of reasonable count rates. In microdiffraction the diffracted beams in the diffraction pattern are discs whose diameters are determined by the convergence angle of the electron probe. The pattern can be indexed in the same manner as for a conventional selected area diffraction pattern.

The main problem with using microdiffraction is that of orienting the sample so that a particle has a prominent zone axis parallel to the electron beam. The most successful way was found to be to tilt the specimen until one of the particles was strongly diffracting, i.e. when it appeared dark in the image. The electron beam was then placed over this particle and focused down to the required diameter. Several attempts must usually be made before a prominent zone axis is found approximately parallel to the electron beam. It is preferable to record several diffraction patterns from a number of particles in order to enable an unequivocal identification of the particle to be made.

The diffraction data obtained from the particles showed that they have cubic symmetry (fig. 6) and an F lattice. An a value of $c.8.0$ Å was determined for the particles from the diffraction pattern. There is no possibility of the patterns being confused with those from the matrix garnet which has $a = 11.93$ Å. The analytical data described in the following section show that the particles are iron-rich, which, coupled with the diffraction data above, suggest that they are magnetite.
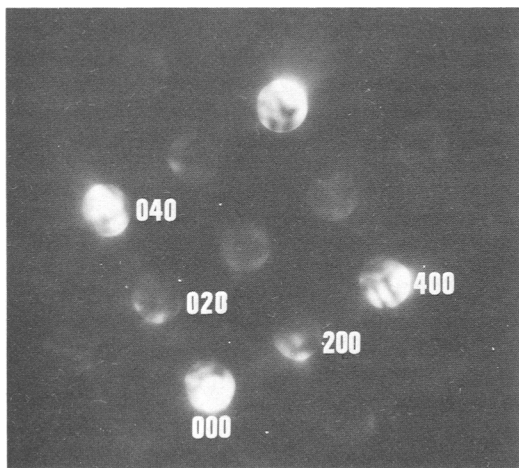
FIG. 6. [100] microdiffraction pattern from magnetite particle within garnet.

There is currently some dispute about the space group of magnetite and spinels in general. Weak 200 reflections commonly occur in the microdiffraction pattern (e.g. fig. 6) although they are forbidden in space group $Fd3m$. Their appearance may be attributed to double diffraction from the first order into the zero order Laue zone as suggested by Smith (1978) and Steeds and Evans (1980) or the fact that the space group of magnetite is $F\bar{4}3m$, and not $Fd3m$ (Grimes et al., 1983).

It is also worth noting here that Cressey (1978) reported the presence of unoriented iron-rich particles in an almandine–pyrope–grossular garnet which he proposed were exsolved almandine. In view of the data presented here and the limitations of the analytical electron microscope (EMMA4) used by Cressey, it seems more likely that his particles were also magnetite. The lack of any crystallographic orientation relationship between two garnets is also very unlikely.

Some particles of quartz have also been identified by AEM in this sample but they are very much less abundant than the magnetite particles. They have similar dimensions to the particles of magnetite, but are usually subhedral with some well-developed faces.

RM5001. In the first ion-thinned samples of thermal garnets from this rock no magnetite particles were found. However, on examining further specimens exsolved particles with an identical morphology to those in sample RM5020 were observed. In comparison the particles are smaller, varying in diameter from 80–250 Å, with the majority being less than 150 Å. A particle density of $\sim 8 \times 10^{15}$ per cm^3 has been determined, a value which is significantly greater than that for the previous sample. However, assuming an average diameter of 160 Å, the volume fraction is 0.17%, which is of the same order of magnitude as sample RM5020. AEM investigations (see following section) have only identified a single phase, in this case magnetite: no quartz has been found.

Magnetite clearly occurs on a localized scale in this sample. After extensive studies, a discontinuity between garnet free of magnetite and garnet containing magnetite was observed in the TEM (fig. 7). The interface is sharp and, in the example here, is delineated by a crack in the sample which probably represents a hiatus in growth of one zone of the garnet. The fracture has probably opened up due to sample preparation or handling of the specimen, but was clearly a pre-existing zone of weakness in the garnet. Approximate crystallographic continuity is maintained across the interface, although there is a slight rotation across the fracture. The *very rapid changes in composition which occur across the thermal garnets, as shown in the
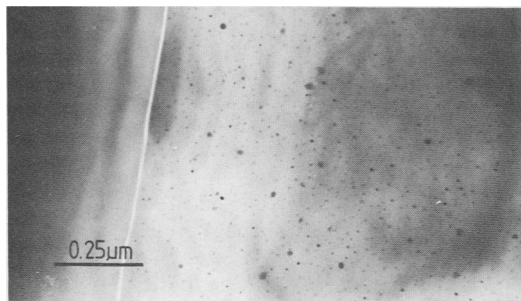
FIG. 7. Electron micrograph of a discontinuity between magnetite-free and magnetite-bearing garnet. The fracture along the boundary between the two regions is probably a discontinuity between periods of growth which has opened up during specimen preparation.

chemical profile fig. 3, allow the exact position of the zone of magnetite in the garnet to be established. The chemical analyses from this region of the garnet (see analysis 5, Table II) show that the interface occurs close to the rim of the garnet, with the magnetite-bearing zone being closer to the core. The composition of the garnet at the discontinuity shown in fig. 7 is indicated in fig. 3 as point Y. From the other investigations it would appear that the actual zone in which magnetite is found is probably not very large. No particles have been observed in any regions of the garnet lying between the core composition and a composition of $al_{67}sp_{21}$ py_4gr_8. This latter composition corresponds to the line X on the analytical profile (fig. 3). It is noticeable that this composition corresponds with

a marked change in the zoning profile for Ca, which is much lower from this point onwards to the rim.

The X and Y therefore delineate a narrow zone in which magnetite exsolution has occurred. All the other areas in the garnet are magnetite-free.

RAS1. Magnetite particles were also observed in these garnets and appear to occur in discrete zones, although it has not been possible to establish their actual spatial distribution with any certainty. The particles in these garnets exhibit a rather broader size range from about 150 up to 400 Å, the largest size of any of the particles observed. Estimation of the particle density gives values of $\sim 1.3 \times 10^{15}$ per cm^3. The volume fraction of the particles was determined to be $\sim 0.75\%$ using an average particle radius of 100 Å (average of fifty-two particle radii). Thus the volume fractions of magnetite in RM5020 and RM5001 are essentially identical.

Analytical electron microscopy

Analytical electron microscopy (AEM) has been used to investigate the chemistry of the exsolved particles and the matrix. Quantitative X-ray microanalysis in the TEM has been carried out using the thin-film approximation of Cliff and Lorimer, 1975 (see Lorimer, 1983, for a recent review). Totals in the analysis must always be normalised to 100% in order to obtain a quantitative analysis because of the ratio technique used. The spatial resolution of the electron probe is of the order of 200 Å for the EM400T operating in the microprobe mode, although 500 Å is often a more realistic value for some very thick specimens due to beam broadening (but see below).

The initial microanalytical investigations on the specimens immediately showed that the exsolved particles were iron-rich in comparison to the matrix garnet. This is illustrated in fig. 8a and b which show EDS X-ray spectra from sample RM5020 for (a) the garnet adjacent to the particle and (b) from the particle itself. In the second spectrum there is a small, but significant, X-ray contribution from the matrix. In RM5020 there is no noticeable decrease in the intensity of the Mn-$K\alpha$ peak, which suggests that Mn is present in the particles as well.

It is inevitable that analyses of very small (< 200 Å) secondary phases will contain significant X-ray contributions from the matrix. The analytical geometries used for microanalysis always result in the matrix phase being present above or below the particle, except perhaps at the very edge of the foil. This is because a typical silicate thin foil has a thickness between 300–1000 Å, generally greater than the size of the particles found in this study.

Table II. AEM analyses of garnet

	1	2	3	4	5
SiO_2	38.45	37.53	37.36	37.86	36.78
Al_2O_3	20.49	21.00	21.29	21.99	22.75
FeO	31.93	31.52	31.39	30.55	31.51
MnO	5.07	5.91	6.06	0.47	0.55
MgO	1.61	1.86	1.70	4.10	3.88
CaO	2.43	2.13	2.18	5.04	4.89
Total	100.00	100.00	100.00	100.00	100.00

Formula based on 12 [O] atoms

	1	2	3	4	5
Si	3.093	3.029	3.016	2.988	2.923
Al	1.943	1.999	2.026	2.046	2.094
Fe	2.148	2.128	2.119	2.016	2.094
Mn	0.345	0.404	0.414	0.031	0.037
Mg	0.193	0.224	0.204	0.480	0.460
Ca	0.209	0.184	0.188	0.424	0.417
Sum	2.897	2.941	2.927	2.953	3.009

Garnet end-members

	1	2	3	4	5
Alm	74.15	72.36	72.41	68.31	69.60
Sp	11.94	13.75	14.14	1.05	1.25
Pyr	6.66	7.62	6.99	16.26	15.30
Gr	7.24	6.27	6.45	14.36	13.86

Analysis 1 - RM5020
Analyses 2 and 3 - RM5001
Analyses 4 and 5 -RAS1
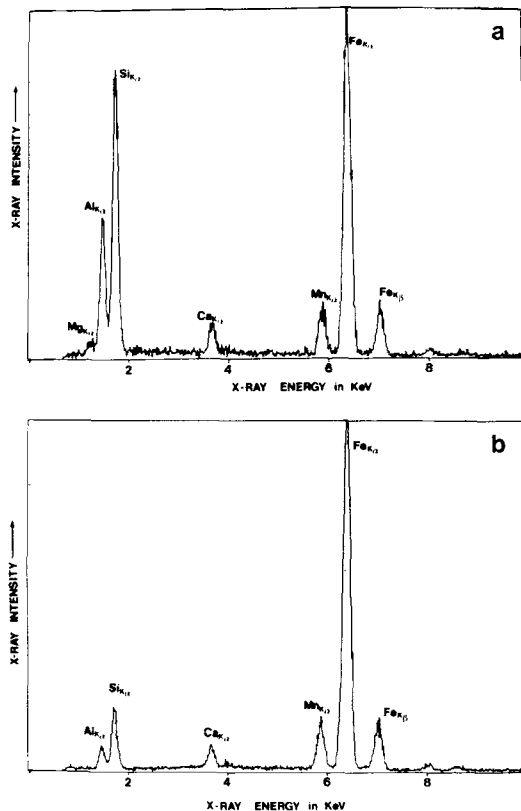
FIG. 8. EDS X-ray spectra of (a) garnet matrix, (b) magnetite particle with small X-ray contribution from the matrix garnet.

The combined effects of matrix X-ray contributions and beam-broadening can be experimentally investigated using Monte Carlo computation techniques of the type described by Michael *et al.* (1984). A Monte Carlo simulation has been carried out for almandine garnet containing iron-rich second-phase particles 300 Å in diameter within a foil 0.1 μm in thickness. The results of this simulation show that with an incident 100 kV electron beam normal to the sample, beam-broadening within the specimen is not a significant problem. Since garnet is a comparatively dense silicate phase, it is reasonable to assume that beam-broadening is not a significant effect in the majority of silicates, even in fairly thick (0.2 μm) thin foils. By far the most important effect is that of X-ray contributions from the matrix containing the particle.

It is evident that single analyses are not capable of giving accurate chemical data from such small second phase particles. However, a recent paper by Cliff *et al.* (1983) provides a simple, but elegant, solution to this problem and enables quantitative data to be obtained. The technique will be outlined briefly here.

If a matrix phase A (garnet) has a high concentration of oxide or element X and oxide Y is preferentially concentrated in the precipitate phase B (magnetite) then analyses of the particle (B) containing contributions from the matrix can be presented graphically against oxide X in the matrix (garnet). This is shown in fig. 9a where analytical data from particles for FeO (oxide Y) in sample RM5020 are plotted against SiO_2 (oxide X). Provided the particle and matrix compositions are fixed, the analytical data plot on a straight line. The effect of increasing the electron path length in the particle is to move the analytical composition along the straight line towards the true particle composition. Thus, although it may in practice (as in this example) be impossible to obtain an uncontaminated analysis of the particle phase, an extrapolation of the straight line will pass through the correct composition of the phase. If there is no oxide Y (SiO_2) in the particle then the intercept of the line on the Y axis gives the concentration of oxide X in the precipitate.

It is necessary to perform in the order of twenty analyses on the particles in order to produce a reasonable extrapolation.

Analytical results

RM5020. Some forty analyses of the particles were made in the TEM as well as several analyses of the garnet matrix using a defocused probe. The garnet analyses and formulae recalculated to 12 oxygen atoms for all three samples are presented in Table II. The TEM analyses usually have good stoichiometry, although there is typically a Y site deficiency of the order of 0.07 cations which is not evident in the equivalent electron probe data. Nevertheless the end-member proportions calculated from both sources are comparable.

The analytical data for the particles are presented in fig. 9a and b. All the elements have been plotted against SiO_2 on the assumption that the magnetite contains no silica. Very clear trends emerge from this analysis and these are summarized below.

(1) SiO_2, Al_2O_3, and MgO all decrease as the contributions from the particle increase.

(2) FeO, MnO, and CaO all exhibit significant increases.

The Y-axis intercept values (i.e. the estimated particle compositions), 2σ values and correlation coefficients for the best fit curves for all three samples are given in Table III. The correlation coefficients for Al and Fe are good, but for Ca, Mg, and Mn are all low, because these three elements
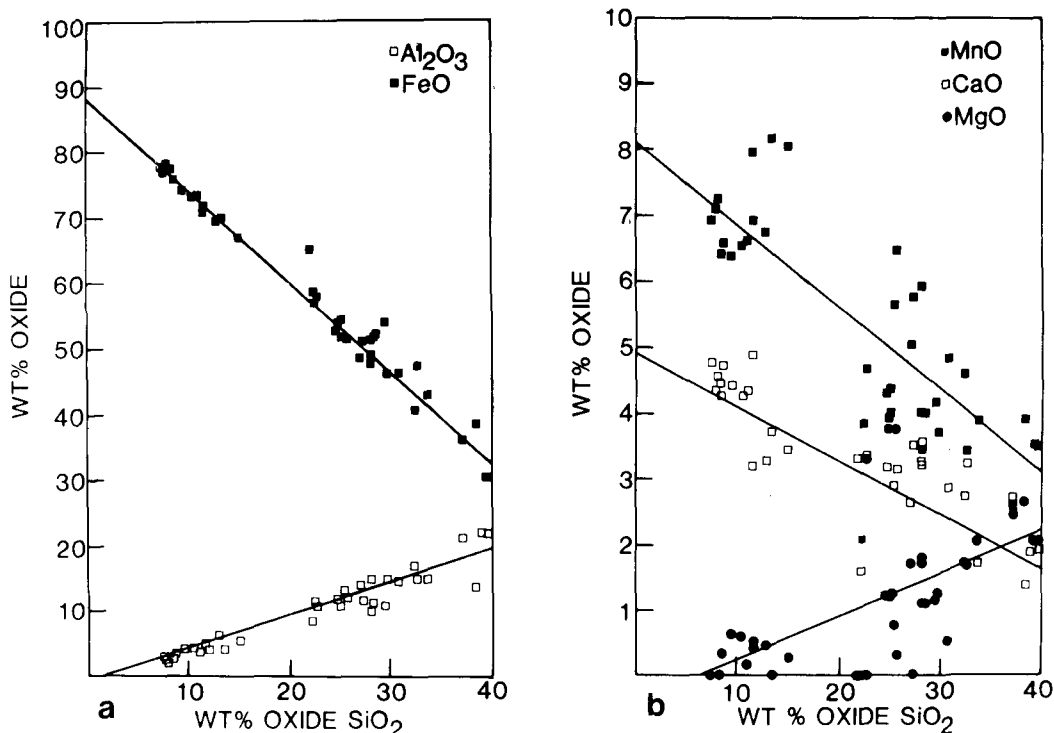
FIG. 9 (a and b). Compositional plots of the analytical data obtained from forty-six particle analyses from sample RM5020. Regression lines for each oxide are shown.

are present in low concentrations in the matrix garnet. A typical particle analysis has a standard deviation of about 20 % for these elements, because of the very low count rates used for the analysis. The compositional variation in the garnet will also contribute to the spread in the data.

The intercept values for the oxides have very large errors, particularly for those elements which are present in low concentrations. The calculated 2σ values for each of the intercepts are high so that no great significance can be placed on the absolute intercept values. Of more importance in such cases is the trend of the data which clearly show a decrease into the particle. The results do, how-

ever, give a reasonable estimate of the particle composition.

RM5001. The data for this sample are considerably different from those for RM5020 and are plotted in figs. 10a and b for twenty-six particles. In contrast to the previous example, only FeO increases as the contribution from the particle increases (the value C = 1.11 for MgO can be ignored because 2σ is too large). All the other elements decrease and are close to zero at their Y intercept (Table III). The particles in this sample can be regarded as being pure magnetite with no other elements present in significant concentrations.

Table III. Intercepts (C), standard deviations (2σ) and correlation coefficients (K) from extrapolation of particle data.

	RM5020			RM5001			RAS 1		
	C	2σ	K	C	2σ	K	C	2σ	K
Al_2O_3	-1.69	3.44	0.95	1.17	5.70	0.90	-3.18	11.49	0.84
FeO	88.80	3.45	-0.98	95.65	4.59	-0.99	102.41	14.93	-0.96
MnO	8.06	1.49	-0.79	1.74	0.88	0.88	0.38	1.72	0.21
MgO	-0.38	1.38	0.60	1.11	2.13	-0.23	-1.62	5.85	0.51
CaO	4.86	1.41	-0.65	0.62	1.03	0.71	0.18	0.74	0.74

Number of analyses used for calculations- RM5020=41;RM5001=26;RAS 1=17.
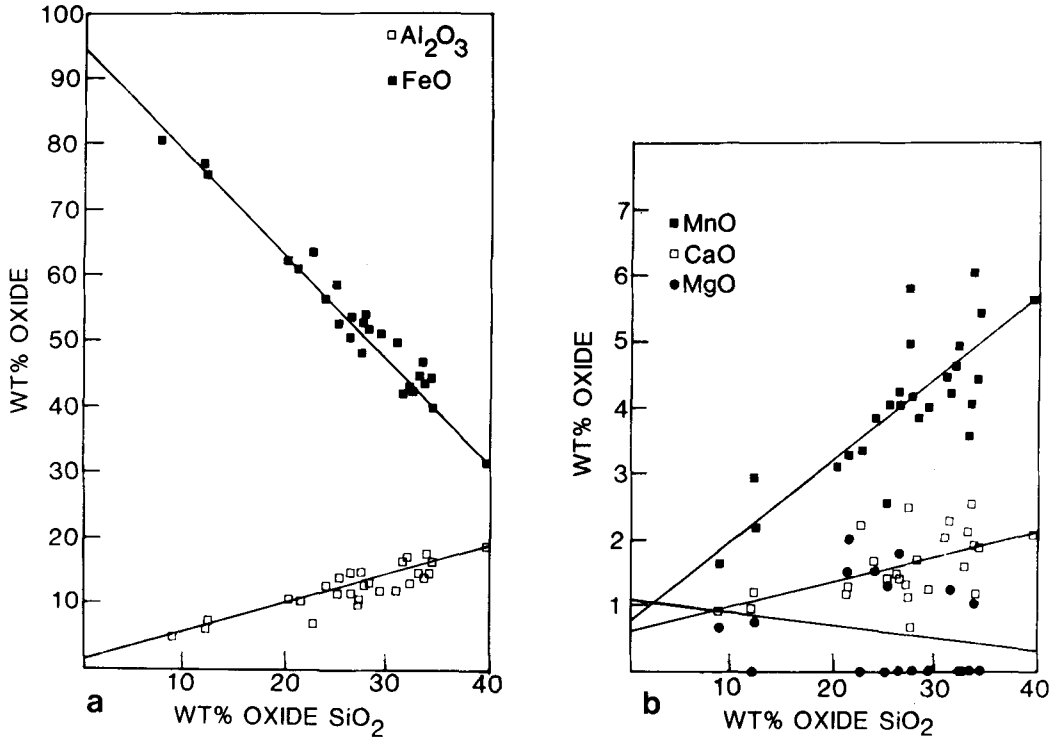
FIG. 10 (a and b). Compositional plots of the analytical data obtained from twenty-six particle analyses from sample RM5001. Regression lines for each oxide are shown.

RAS1. Seventeen particle analyses were made of this garnet. The data are presented in fig. 11a and b. Only Fe increases as the contribution from the particles increases. This suggests that, as for RM5001, the particles are almost pure magnetite. The extrapolated total of 102.41 wt. % FeO has a large error of ±14.93% mainly due to the limited number of data points (17) used in the extrapolation of which only one has low SiO$_2$ concentration.

Origin of the particles

There appear to be two possibilities for the origin of the magnetite particles within the garnets. They may be inclusions which are incorporated into the garnet during growth or, alternatively, they are particles exsolved during the cooling of the rocks. The latter explanation is favoured here for the following reasons. The particles are anomalously small in size for crystals which were incorporated into the garnet during prograde growth. A significant degree of coarsening of the particles could reasonably be expected if the garnets had been held

at elevated temperatures for a considerable time. This is not evident. It is also found that inclusions of other phases within the garnet vary in size from about 10 μm (for rutile inclusions) up to 50 μm for inclusions of quartz. It seems improbable that such a large difference in inclusion size is likely to be found, the magnetite particles being about 3 orders of magnitude smaller. Furthermore, the spatial distribution of the particles does not correspond to the zones in the garnet which contain abundant inclusions of quartz, etc. It is these zones which correspond to the periods of most rapid growth and would therefore be the most likely to contain inclusions of magnetite.

Exsolution mechanism

The morphology and mode of occurrence of the particles is consistent with a mechanism of heterogeneous nucleation at defects within the garnet. Homogeneous nucleation is ruled out because of the lack of orientation relationships. In any case homogeneous nucleation can only occur between phases with very similar crystal structures. The
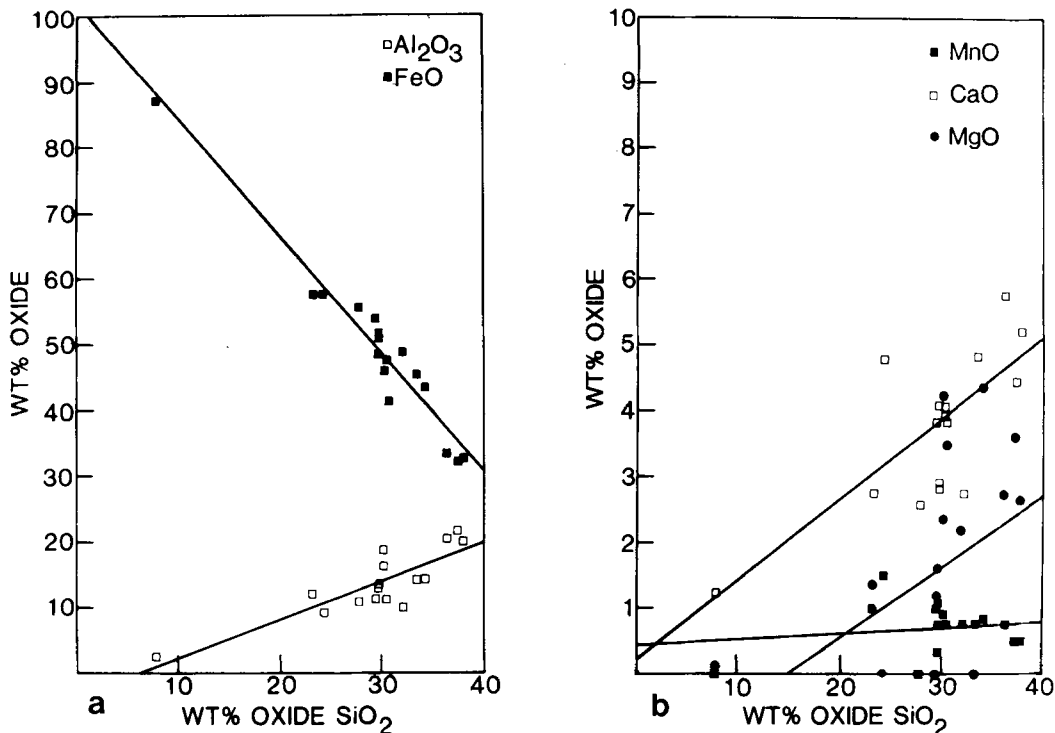
FIG. 11 (a and b). Compositional plots of the analytical data obtained from seventeen particle analyses from sample RAS1. Regression lines for each oxide are shown.

garnets in the study have exceptionally low dislocation densities; therefore vacancy clusters probably play a much more significant role as nucleation sites. The spherical shapes of the precipitates and their random orientations within the matrix indicates that there is no structural similarity between the two phases on any plane. The two phases therefore have a completely incoherent relationship across the interface from the nucleation stage. The particles are spherical in order to minimize the surface area and hence the surface free energy.

This state of incoherency and the lack of any crystallographic relationship between particle and matrix is unusual, if not unique, in nature. To our knowledge there are no documented examples of exsolved phases whose orientation is not in any way crystallographically controlled by the host phase, either in metals or minerals.

Incoherency between the phases is likely only when there is a large volume difference between the phases. Chadwick (1972) suggests, in the case of metals, that the interface will be semicoherent when the volume difference between the phases lies

between 5 and 25%. Above this value it is argued that there is no real registry between the lattices and the interface is incoherent. For the case of magnetite exsolved in garnet the volume difference is about 14% (based on volumes per oxygen atom), but the phases are clearly incoherent. The upper value quoted by Chadwick for loss of semicoherency is an estimate because, as mentioned above, no examples of incoherent nucleation have been observed and this value may therefore be inaccurate.

Although all three samples contain exsolved magnetite there are some compositional complexities evident in the exsolved particles from RM5020. The exsolution of magnetite in samples RM5001 and RAS1 will be discussed initially because it appears to be somewhat simpler. Some of the following comments do, however, apply to all three samples.

The electron microprobe analyses of garnets from all three samples do not exhibit any marked departures from stoichiometry when total Fe is calculated as Fe^{2+} that might be indicative of the presence of significant quantities of Fe^{3+}. Never-

theless, it is abundantly clear that there is sufficient Fe^{3+} for the exsolution of magnetite to occur during the cooling history of the garnet but the actual concentrations are clearly low as can be seen from the low volume fraction of the particles (0.7 %). Furthermore, the calculated volume fractions, given the approximations involved, are very similar. A possible mechanism for the exsolution process is discussed below.

Fe^{3+} is commonly assumed to substitute for Al in sixfold co-ordination in garnets of the pyralspite series. The radius of the Fe^{3+} ion is considerably larger (0.49 Å) than the Al^{3+} ion (0.39 Å) (ionic radii from Shannon and Prewitt, 1969) for which it substitutes. At high temperatures expansion of the crystal structure enables Fe^{3+} to be successfully accommodated in octahedral co-ordination without excessive distortion of the lattice. As cooling proceeds the crystal structure contracts with a resultant increase in distortion and strain around the Fe^{3+} cation. Once the activation energy for nucleation of magnetite has been exceeded exsolution will commence. Incoherent exsolution can only occur when a significant degree of undercooling has taken place. Two of the samples (RM5020 and RAS1) formed at temperatures below 550 °C, so that exsolution can only have commenced below this temperature, but it is difficult to assess ΔT. It is possible that it was as much as 50 °C.

A possible reaction can be considered simplistically in terms of exsolution of magnetite from pure almandine assuming that 1% of the Al in octahedral co-ordination is substituted by Fe^{3+}, i.e.

$$Fe_3Al_{1.98}Fe^{3+}_{0.02}Si_3O_{12} = 0.01FeO \cdot Fe_2O_3 +$$
$$0.99Fe_3Al_2Si_3O_{12} + 0.02FeO + 0.03SiO_2.$$
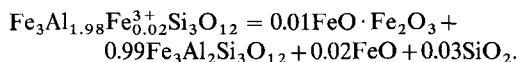
The volume fraction of magnetite produced in this reaction (0.3 %) is consistent with the observed volume fraction in the garnets.

The most obvious problem with the proposed reaction is the production of SiO_2 and FeO. Although quartz has been found as discrete particles in one of the samples (RM5020), none occurs in the garnets that have exsolved almost pure magnetite. An analogous situation has been observed by Champness (in prep.) in metamorphic olivines which have exsolved magnetite as platelets, but show no evidence of any exsolved quartz as a reaction product. The implications of these observations are that cations can sometimes substitute in sites where they would not normally be expected, perhaps only in small quantities. A further example of such a phenomenon has been observed by Ashworth (1979) in chondritic olivine in which Cr^{3+} appears to substitute for Si, despite its usual preference for octahedral co-ordination. It is thus possible that Fe^{3+} can substitute for Si as well as Al

in pyralspite garnets. Certainly this substitution is well known in schorlomite and melanite garnets where Fe^{3+} and Al^{3+} substitute for Si^{4+} when Ti^{4+} occurs in octahedral co-ordination, although in the garnets studied here no Ti has been detected by microprobe analysis. If Fe^{3+} is present in tetrahedral sites charge balance must be maintained by introducing oxygen vacancies into the structure. A possible balanced reaction can only be constructed if it is assumed that $Fe^{3+}(IV)$ is $> Fe^{3+}(VI)$ as below.

$$Fe_3(Al_{1.99}Fe^{3+}_{0.01})Si_{2.985}Fe^{3+}_{0.015}O_{11.99} =$$
$$0.0125FeO \cdot Fe_2O_3 + 0.995Fe_3Al_2Si_3O_{12} +$$
$$0.0025FeO.$$
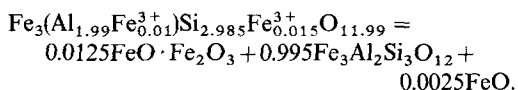
The residual FeO is only a minute quantity and may be involved in an oxidation reaction with water in the garnet. It is well established that nominally anhydrous phases contain water in low quantities and garnet is no exception. Aines and Rossman (1984) report concentrations ranging between 0.02 and 0.25 wt. % in garnets of the pyralspite series, clearly sufficient to provide a source of oxygen for the reaction. The second reaction can simply be described as:

$$FeO + \tfrac{1}{3}H_2O = \tfrac{1}{3}FeO \cdot Fe_2O_3 + \tfrac{1}{3}H_2.$$
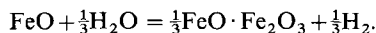
Hydrogen released from this reaction will be readily lost from the garnet by volume diffusion. This appears to be the best model to account for the occurrence of pure magnetite in samples RM5001 and RAS1 in the absence of quartz. More simply it is also possible that the magnetite is non-stoichiometric.

The chemical data suggest that the composition of the exsolved phase in RM5020 is different from that in the other two samples. Ca and Mn are found in considerable quantities in the particles and discrete SiO_2 particles also occur. Although Mn could be present as jacobsite ($MnFe_2O_4$) in solid solution in the magnetite, the occurrence of Ca in the particles is not so readily explained. It is possible that Ca is concentrated in a stranded diffusion profile around the particle. As the particle develops, Ca and Mn must diffuse away from the growing particle. If diffusion does not take place sufficiently rapidly, Ca and Mn will become concentrated in the garnet on the margins of the particle. There are, however, considerable problems with this explanation and it cannot be regarded as being satisfactory. Of all the samples studied, RM5020 is likely to have had the longest cooling history and preservation of a diffusion profile on these grounds alone seems improbable. Furthermore the most likely sample to have preserved evidence of a chemical profile, RM5001, contains no evidence of such a feature.

Alternatively Ca may be present within the magnetite particle in solid solution, but the nature of the Ca-bearing phase is obscure. At present there does not appear to be a satisfactory solution to this problem.

Interpretation of particle size

Each of the garnets examined have different particle densities and the particles cover different size ranges. There are two main factors which determine the size of the exsolved particles. These are (a) the rate of diffusion of species to and from the growing particle which is controlled by the cooling history (dT/dt) of the rock, and (b) the original Fe^{3+} content of the garnet. It is difficult to establish which of these factors played the more important role in determining the final size of the particles. However, because the volume fractions are comparable in each sample it seems most probable that the differences in particle size and density are best explained by differences in the cooling histories of the rocks. The particles will undergo coarsening once initial nucleation and growth have occurred, with the larger particles coarsening at the expense of the smaller ones. Thus the particle size will increase as the particle density decreases. For example samples RM5020 and RAS1 both have lower particle densities and larger grain sizes than sample RM5001 from the contact aureole. Clearly coarsening of the particles could not take place in the latter sample due to its comparatively rapid cooling history. The larger particle size and lower particle density in RM5020 and RAS1 is consistent with resorbtion of the smaller particles as the larger particles coarsen. It is also possible that the lower volume fraction of magnetite in RM5001 is due to incomplete exsolution of Fe^{3+} as a result of rapid cooling.

Occurrence of Fe^{3+}-rich zones in garnet

The occurrence of discrete zones of Fe^{3+}-enrichment encountered in sample RM5001 may result from two possible causes. The first is simply that rapid growth results in the incorporation of more Fe^{3+} ions into the structure of garnet than would occur during slow growth. This is likely to arise because the decrease in free energy resulting from the formation of a stable, ordered crystal is significantly greater than the free energy increase imposed by the incorporation of foreign ions into the structure. The rate of growth may be responsible for the occurrence of Fe^{3+} in tetrahedral co-ordination in RM5001 and RAS1 and not in RM5020. Periods of rapid growth during prograde metamorphism result in anomalous substitutions which might not

occur during equilibrium growth. Certainly the thermal contact garnet studied (RM5001) is likely to have grown very rapidly at high temperatures, a condition which would favour this substitution. Joesten (1983) has demonstrated that grain growth under non-isothermal conditions in contact aureoles is initially very rapid for a short period of time, after which growth ceases. The rate of change of diameter with time is greatest at the very earliest stages of growth which, if the above supposition is correct, should mean that Fe^{3+} will be present in the cores of the garnets, provided it is present in the fluid phase. However, no magnetite has been observed in the core region of the garnet, but it does occur in an outer zone of the garnet where the rate of growth will have been somewhat slower. This implies that the presence of Fe^{3+} in garnet is dominated by the redox potential of the fluid around the growing garnet. The presence of Fe^{3+}-bearing zones may well be a sensitive indicator of reactions which control f_{O_2} during prograde metamorphism. There is also evidence to suggest that progressive reduction during metamorphism does not necessarily take place. Rather, f_{O_2} can change abruptly as different divariant equilibria are encountered in P–T–f_{O_2} space as shown by Greenwood (1975).

Conclusions

Transmission electron microscopy has shown that metamorphic almandine garnets contain myriad particles of magnetite which have exsolved during cooling. We conclude that the Fe-rich particles found by Cressey (1978) in a pyrope-almandine–grossular garnet are also magnetite, not another garnet as he suggested.

The particles are found to have a completely incoherent and unoriented relationship with the host phase. Analytical data demonstrate that, although two of the samples contain essentially pure magnetite particles, the particles in a third sample have a very unusual chemistry with high Mn and Ca contents. There is at present no satisfactory explanation for this phenomenon.

Quartz is only found to be an important exsolution reaction product in two of the samples and leads to the conclusion that, under certain growth conditions, Fe^{3+} can substitute for Si^{4+} in tetrahedral co-ordination.

The sizes of the exsolved particles is probably a qualitative indicator of the cooling rate of the garnet because the Fe^{3+} contents of the garnets are probably very similar in the first instance. It is probable that the difference in sizes between exsolved particles in contact and regional garnets does reflect differences in cooling rates, with

coarsening occurring in the regional garnets to a greater extent.

Finally the occurrence of discrete zones which contain magnetite particles is an indicator of changing f_{O_2} of the fluid phase during prograde metamorphism. These changes must be abrupt and are due to the operation of different buffering reactions during the metamorphic history.

REFERENCES

Aines, R. D., and Rossman, G. R. (1984) *Am. Mineral.* **69**, 1116-26.

Ashworth, J. R. (1979) *Mineral. Mag.* **43**, 535-8.

Atherton, M. P. (1977) *Scott. J. Geol.* **13**, 331-70.

Barber, D. J. (1970) *J. Mater. Sci.* **5**, 1-8.

Bosworth, T. O. (1910) *Q. J. Geol. Soc.* **66**, 376.

Brearley, A. J. (1984) *Petrological and electron optical studies of metamorphic reactions.* Ph.D. thesis. Univ. of Manchester.

Chadwick, G. A. (1972) *Metallography of phase transformations.* Butterworths.

Champness, P. E., and Lorimer, G. W. (1971) *Contrib. Mineral. Petrol.* **33**, 171-83.

Cliff, G., and Lorimer, G. W. (1975) *J. Microsc.* **103**, 203-7.

—— Powell, D. J., Pilkington, R., Champness, P. E., and Lorimer, G. W. (1983) *Inst. Phys. Conf. Ser.* No. 68. 63-6.

Cressey, G. (1978) *Nature,* **271**, 533-4.

Greenwood, H. J. (1975) *Am. J. Sci.* **275**, 573-93.

Grimes, N. W., Thompson, P., and Kay, H. F. (1983) *Proc. R. Soc. Lond.* **A386**, 333-45.

Hollister, L. S. (1969) *Geol. Soc. Am. Bull.* **80**, 2465-94.

Joesten, R. (1983) *Am. J. Sci.* **283A**, 233-54.

Lorimer, G. W. (1983) *X-ray microanalysis.* In *Quantitative Electron Microscopy.* Proc. of Institute of Physics—NATO 25th Scottish Universities Summer School in Physics.

MacKenzie, W. S., and Guilford, C. (1981) *Atlas of rock-forming minerals.* Longmans, London.

Michael, J. R., Cliff, G., and Williams, D. B. (1984) *Scanning Electron Microscopy,* **4**, 1697-705.

Mongkoltip, P., and Ashworth, J. R. (1983) *Am. Mineral.* **68**, 143-55.

Moseley, D. (1981) Ibid. **66**, 976-9.

——(1984) Ibid. **69**, 139-53.

Shannon, R. D., and Prewitt, C. T. (1969). *Acta Crystallogr.* **25**, 925-46.

Smith, P. P. K. (1978) *Phil. Mag.* **38**, 99-102.

Steeds, J. W., and Evans, N. S. (1980) Proc. 38th EMSA Meeting, 188-91.